Materials Today Bio 21 (2023) 100685

Contents lists available at ScienceDirect

Materials Today Bio

journal homepage: www.journals.elsevier.com/materials-today-bio

A bioactive microparticle-loaded osteogenically enhanced bioprinted scaffold that permits sustained release of BMP-2

Ji Min Seok [a,b,1], Min Ji Kim [c,1], Jin Ho Park [d,e], Dahong Kim [b], Dongjin Lee [a], Seon Ju Yeo [a], Jun Hee Lee [a], Kangwon Lee [b,f], June-Ho Byun [d,e,***,2], Se Heang Oh [c,**,2], Su A Park [a,*,2]

[a] Nano-Convergence Manufacturing Systems Research Division, Korea Institute of Machinery and Materials (KIMM), Daejeon, 34103, Republic of Korea
[b] Department of Applied Bioengineering, Graduate School of Convergence Science and Technology, Seoul National University, Seoul, 08826, Republic of Korea
[c] Department of Nanobiomedical Science & BK21 FOUR NBM Global Research Center for Regenerative Medicine, Dankook University, Cheonan, 31116, Republic of Korea
[d] Department of Oral and Maxillofacial Surgery, Gyeongsang National University School of Medicine and Gyeongsang National University Hospital, Jinju, 52727, Republic of Korea
[e] Department of Convergence Medical Science, Gyeongsang National University, Jinju, 52727, Republic of Korea
[f] Research Institute for Convergence Science, Seoul National University, Seoul, 08826, Republic of Korea

ARTICLE INFO

Keywords:
Bioprinting
BMP-2
Microparticle
Scaffold
Sustained release

ABSTRACT

Extrusion-based bioprinting technology is widely used for tissue regeneration and reconstruction. However, the method that uses only hydrogel as the bioink base material exhibits limited biofunctional properties and needs improvement to achieve the desired tissue regeneration. In this study, we present a three-dimensionally printed bioactive microparticle-loaded scaffold for use in bone regeneration applications. The unique structure of the microparticles provided sustained release of growth factor for $>$ 4 weeks without the use of toxic or harmful substances. Before and after printing, the optimal particle ratio in the bioink for cell viability demonstrated a survival rate of $\geq$ 85% over 7 days. Notably, osteogenic differentiation and mineralization—mediated by human periosteum-derived cells in scaffolds with bioactive microparticles—increased over a 2-week interval. Here, we present an alternative bioprinting strategy that uses the sustained release of bioactive microparticles to improve biofunctional properties in a manner that is acceptable for clinical bone regeneration applications.

1. Introduction

Bioprinting is widely used in tissue engineering and biomedical applications [1–3]. The main advantage of three-dimensional (3D) printing strategies is that they enable personalized fabrication of large defect regions in patients who require regeneration within complex structures [4]. An important consideration is the expansion of bioinks available for successful scaffold fabrication [5,6]. Sodium alginate (SA) is a natural substance that is biodegradable under normal physiological conditions; it is commonly used as a bioink to fabricate engineered tissues, such as vessels [7], muscles [8], cartilages [9], nerves [10], hearts [11], and bones [12]. Because SA exhibits stable printability and is rapidly crosslinked by divalent cations, it readily encapsulates and can print cells at a high density while maintaining cell viability [13,14]. However, it has been difficult to incorporate cell moieties into SA hydrogel networks [15,16]. Because the hydrophilicity of SA facilitates mixing with other materials, composites of SA with bioactive materials have been extensively studied to improve its biofunctional properties [17,18].

Common material types that demonstrate superior osteogenesis in bone tissue engineering applications include natural and synthetic polymers, bioceramics, biodegradable metals, and nanomaterials [19]. Controlled delivery of drugs, physiologically active biomolecules, and signaling substances to tissues that require regeneration has also been demonstrated [20]. However, because of the low bioavailability and

* Corresponding author.
** Corresponding author.
*** Corresponding author. Department of Oral and Maxillofacial Surgery, Gyeongsang National University School of Medicine and Gyeongsang National University Hospital, Jinju, 52727, Republic of Korea.
E-mail addresses: surbyun@gnu.ac.kr (J.-H. Byun), seheangoh@dankook.ac.kr (S.H. Oh), psa@kimm.re.kr (S.A. Park).
[1] These co-authors have made equal contributions to this work.
[2] These corresponding authors have made equal contributions to this work.

https://doi.org/10.1016/j.mtbio.2023.100685
Received 25 January 2023; Received in revised form 3 May 2023; Accepted 29 May 2023
Available online 13 June 2023

short half-life of osteoinductive protein, a periodic delivery system is essential for the achievement of effective drug activity [21]. One strategy for bone regeneration is the sustained release of a growth factor, such as bone morphogenetic protein-2 (BMP-2). This approach has been extensively studied for various drug delivery systems, including microneedle patches, injectable devices, micro- and nanoparticles, and hydrogels [22]. The growth factor is either physicochemically loaded into the hydrogel or coated onto the surfaces of particles and devices, then delivered to the tissue defect. However, because harmful solvents and chemicals are used in this process, it may be difficult to ensure biological stability for clinical purposes. To overcome this limitation, we previously established a clinically applicable drug delivery system that could physically load growth factor onto the surface of a unique leaf-stacked structure (LSS), which then achieved sustained release of bioactive molecules [23–26]. Here, we report the novel bioprinting of LSS microparticles to provide effective osteogenic function for bone regeneration. We prepared a maze-like structure on medical-grade polycaprolactone (mPCL) microparticles without physical/chemical modification; growth factor delivery was continuously achieved because of the large surface area formed. To our knowledge, few studies have been reported regarding the bioprinting of such clinically applicable growth factor-loaded microparticles for sustained-release delivery. Furthermore, our approach to encapsulate entire leaf-stacked structure (ELSS) microparticles and stem cells in SA bioink enables sustained release of BMP-2 and suitable bioprintability while ensuring scaffold shape fidelity. This process can be controlled by the ratio of ELSS microparticles to SA bioink and regulated by the growth factor loading concentration, thus inducing osteogenic differentiation of responsive cells. Additionally, we examined the interactions of human periosteum-derived cells (hPDCs) with composite fabricated from growth factor-loaded microparticles and a bioprintable hydrogel by characterizing the ELSS-loaded SA bioink and performing standard assays that focused on the osteogenic biological response of encapsulated cells.

2. Materials and methods

2.1. Materials

mPCL (M_w = 80,000 Da; Evonik, USA) and tetraglycol were used to fabricate ELSS particles. SA was used to prepare $CaCl_2$-crosslinked bioink. Albumin (bovine serum albumin; BSA)-fluorescein isothiocyanate conjugate (FITC-BSA; Sigma–Aldrich, USA) was used as a model protein; recombinant human BMP-2 (Chinese hamster ovary cell line; R&D Systems, USA) was used to induce osteogenic differentiation in target cells. All other reagents and materials used in experiments were purchased from Sigma–Aldrich.

2.2. Preparation of ELSS microparticles

mPCL-based ELSS microparticles were fabricated using a heating/cooling method as previously described [23,24]. mPCL powder was dissolved at 90 °C in tetraglycol at 15 wt%; the heated mPCL solution was immediately cooled in the refrigerator at 4 °C for 1 h to induce polymeric precipitation with a leaf-stacked structure. The polymer precipitate (ELSS particles) was thoroughly washed with water, separated using standard testing sieves (aperture diameters: 100–300 μm), and lyophilized. ELSS microparticle morphology was observed using a scanning electron microscope (S-4300, Hitachi, Japan) located at the Center for Biomedical Engineering Core Facility. ELSS microparticles were used for *in vitro* cell culture after they had been sterilized with ethylene oxide.

2.3. Preparation of ELSS microparticle-loaded SA bioinks

A solution of 3% SA was prepared in Dulbecco's modified Eagle's medium (DMEM; Gibco, USA), which based on our previous studies that investigated the printability of alginate according to its concentration [31,32]. ELSS microparticles were mixed in 3% SA at loading rates of 0, 1, 3, and 5 wt%, respectively. Each mixture was precrosslinked with 1% $CaCl_2$, then gently mixed using a spatula to form ELSS ink (Table 1). All ink preparation processes were performed on a sterilized bench at room temperature.

Table 1
ELSS ink identification.

ELSS microparticle content (wt%) in sodium alginate (SA) solution	Acronym
0	ELSS0
1	ELSS1
3	ELSS3
5	ELSS5

2.4. Printability and rheological properties of ELSS-loaded SA bioinks

A laboratory-made 3D printing system at the Korea Institute of Machinery and Materials was used to evaluate the printability of ELSS microparticle-loaded inks [27]. The distribution of ELSS microparticles in each ink was determined by optical microscopy (BX51; Olympus, Japan). Printability was assessed by regulating the nozzle gauge (21G–23G), printing speed (30–120 mm/min), and printing pressure (90–360 kPa). For investigation of the stable printable range within the regulated printing parameters, the spreading ratio of the printed strand was measured using the optical microscope and classified into four types according to strand fidelity [28]: unprinted flow, unstable flow, stable flow, and overflow.

$$Spreading\ ratio = \frac{Printed\ strand\ diameter\ (B)}{Nozzle\ diameter\ (A)}$$

The rheological properties of each ELSS microparticle-loaded ink were determined using a rheometer (TA Instruments, USA) in frequency sweep mode over the frequency range of 0.1–10 Hz at 1% shear strain, with a plate geometry of 40 mm diameter and 1 mm gap. The mean mesh size (ξ) of each ELSS microparticle-loaded ink was calculated from the storage modulus (G′) and rubber elasticity theory as follows [29]:

$$Mean\ mesh\ size\ (\xi) = \left(\frac{G' N_A}{RT}\right)^{-1/3}$$

where N_A is Avogadro's constant, R is the molar gas constant, and T is the temperature.

2.5. Fabrication and characterization of 3D printed scaffolds with ELSS-loaded SA bioinks

Based on the characterization of ELSS microparticle-loaded inks, we fabricated scaffolds using the 3D printing system described in Section 2.4. Images of the fabricated scaffolds were obtained using a digital camera after samples had been printed with the following dimensions: 20 × 20 × 4 mm^3. The surface morphologies of the scaffolds were determined using samples that had been lyophilized at −85 °C for 24 h in a freeze-dryer (Il Shin Biobase, Korea). After the scaffold samples had been prepared for scanning electron microscope imaging, the strand surface of each scaffold was observed at magnifications of 60 × and 250 × . The morphologies of ELSS microparticles in scaffolds were observed at 2500 × magnification. The chemical compositions of the scaffolds were established by Fourier-transform infrared spectroscopy (Alpha; Bruker, Germany) over the range of 4000–600 cm^{-1} at a resolution of 1 cm^{-1}.

2.6. Release of BMP-2 from BMP-2-loaded ELSS microparticles in ELSS-loaded SA bioinks

BMP-2 was immobilized in ELSS microparticles using the procedures described above for FITC-BSA. A syringe was filled with 1 mL of the solution of ELSS microparticles and BMP-2 (1 and 10 μg/mL of BMP-2 in phosphate-buffered saline [PBS] supplemented with 1% BSA). BSA was added to prevent the degradation or inactivation of BMP-2 [30]. The amount of BMP-2 loaded in ELSS microparticles was quantified via direct enzyme-linked immunosorbent assays (Duoset, R&D Systems) [33]. To observe the release behavior of BMP-2 from ELSS microparticles, BMP-2-loaded ELSS microparticles (10 mg) were incubated in 1 mL of 1% BSA in PBS; they were incubated at 37 °C for 28 days with shaking at 50 rpm. The incubated media were collected at 24-h intervals and replaced with fresh PBS. The amount of BMP-2 released from each particle was detected using the enzyme-linked immunosorbent assay kit, in accordance with the manufacturer's protocol.

FITC-BSA was loaded into ELSS microparticles to confirm that growth factor-loaded ELSS microparticles remained in the scaffolds after printing. First, syringes were filled with ELSS microparticles (1 mL) and FITC-BSA solution (1 mg/mL in PBS [pH ~7.4]). Syringes containing LSS particles/FITC-BSA solution were stored at 4 °C for 3 h under positive pressure to allow the FITC-BSA solution to infiltrate porous ELSS microparticles. Then, the excess solution was aspirated and lyophilized. Second, the FITC-BSA-immobilized ELSS microparticles were gently mixed with 3% SA, then precrosslinked with 1% $CaCl_2$ to enable extrusion. Finally, printing was carried out in a grid pattern according to the results of ELSS ink printability tests. The distribution of ELSS microparticles in the SA ink and release pattern of FITC-BSA from ELSS particles in PBS with 0.1% $CaCl_2$ were imaged over 14 days using a fluorescence microscope (ECLIPSE-Ti; Nikon, Japan).

2.7. Cell culture and preparation of ELSS-loaded SA bioinks

To evaluate cell viability after encapsulation in an ELSS ink and subsequent printing, MC-3T3-E1 osteoblast-like cells were cultured in DMEM with 10% fetal bovine serum (Gibco) and 1% penicillin–streptomycin (Gibco); cells were grown in a cell incubator (Thermo Fisher Scientific, USA) at 5% CO_2 and 37 °C until they reached 90% confluence. Primary cultures of hPDCs were conducted under identical conditions. For hPDC culture, periosteal tissues were obtained in accordance with a protocol that had been approved by the Institutional Review Board of Gyeongsang National University Hospital (approval no. GNUHIRB 2014-05-012). Periosteal explants (5 × 20 mm^2) were harvested from a patient's mandible during the surgical extraction of impacted lower third molars. hPDCs were isolated as previously described [34,35]. Briefly, periosteal tissues were cultured in 100-mm-diameter culture dishes in DMEM with 10% fetal bovine serum, 100 IU/mL penicillin, and 100 μg/mL streptomycin; incubation was performed at 37 °C in 95% humidified air and 5% CO_2. When cells reached 90% confluence, adherent cells were passaged by gentle trypsinization and reseeded in fresh medium. This process was repeated three times to obtain stable cultured cells.

An ELSS bioink was fabricated using a cell suspension prepared in DMEM. The ink, which was prepared with ELSS microparticles at 0, 1, 3, and 5 wt%, had a density of 3 × 10^6 cells/mL. After the ELSS bioink had been printed, scaffolds were cultured under the conditions described for cell culture. Osteogenic differentiation, mineralization, and immunocytochemical analysis of cells in scaffolds were determined by exchanging the culture medium with minimum essential medium alpha (Gibco) osteogenic differentiation medium containing 10% fetal bovine serum, 1% penicillin–streptomycin, 100 nM dexamethasone (Sigma–Aldrich), 50 μM L-ascorbic acid (Sigma–Aldrich), and 10 mM β-glycerophosphate disodium salt hydrate (Sigma–Aldrich).

2.8. Cell viability after bioprinting of ELSS-loaded SA bioinks

The viabilities of cells encapsulated in scaffolds were evaluated over 7 days using a live/dead cell assay kit (Life Technologies, USA). Calcein AM and ethidium homodimer-1 were used to stain cells in scaffolds for 30 min in an incubator, in accordance with the manufacturer's instructions. Stained cells were observed using a fluorescence microscope; live cells were green and dead cells were red.

2.9. Osteogenic differentiation of hPDCs in scaffolds

The osteogenic differentiation of hPDCs in scaffolds was examined over 14 days using an alkaline phosphate (ALP) assay kit (Takara, Japan). To remove alginate from scaffolds, the cultured scaffolds were immersed in filtered 0.5 M ethylenediaminetetraacetic acid (Invitrogen, USA), then centrifuged (MF550; Hanil Scientific, South Korea) at 1300 rpm for 3 min. After removal of the supernatant, the ELSS bioink was washed three times with PBS. hPDC lysates were collected in radioimmunoprecipitation assay buffer (Thermo Fisher Scientific). In accordance with the ALP assay kit protocol, the absorbances of prepared samples were measured at 405 nm using a multimode microplate reader (SpectraMax iD3; Molecular Devices, USA).

2.10. Mineralization of hPDCs in scaffolds

OsteoImage mineralization assays (Lonza, Switzerland) were conducted after 1 or 2 weeks of growth to evaluate hPDC mineralization in scaffolds. After hPDCs had been fixed in 4% paraformaldehyde, cell nuclei were labeled with 4′,6-diamidino-2-phenylindole (DAPI) (1:2000; Vector Laboratories, USA) for 45 min and scaffolds were stained with Alizarin Red (40 mM, Sigma–Aldrich) for 1 h at room temperature; these steps were followed by three washes in PBS. Stained samples were observed by digital microscopy (ViTiny, USA). Calcium assays were carried out using the QuantiChrom calcium assay kit (BioAssay Systems, USA) to evaluate the rate of calcium deposition in scaffolds. The absorbances of prepared samples were measured at 612 nm using a multimode microplate reader, in accordance with the manufacturer's instructions.

2.11. Immunocytochemical analysis of hPDCs in scaffolds

After incubation in cell culture for 1 or 2 weeks, hPDCs suspended in ELSS microparticle-loaded alginate hydrogels were fixed in 4% paraformaldehyde for 20 min at 4 °C, then permeabilized with 0.1% Triton X-100 and blocked with 10% BSA. Cells were incubated with an anti-Runx2 primary antibody (1:100; Abcam, USA) for 12 h at 4 °C, then with Alexa Fluor 488 secondary antibody (1:200; Abcam) for 1 h at room temperature. Stained cells were observed using a confocal laser microscope (LSM 700; Carl Zeiss, Germany).

2.12. Statistical analysis

All data are presented as means ± standard deviations. Statistical analysis was carried using one-way analysis of variance with Tukey's *post hoc* test. The significance level was set at $P < 0.05$.

3. Results and discussion

3.1. Fabrication and characterization of ELSS microparticles

Porous ELSS microparticles were fabricated by simple heating/cooling of PCL in tetraglycol solvent. Because tetraglycol is not a good solvent for PCL at room temperature, the PCL solution was prepared at moderately high temperature (90 °C). During the cooling step, micron-sized ELSS microparticles spontaneously formed due to the low solubility of

PCL in tetraglycol at 4 °C. The transparent solution in the hot state turned into an opaque paste with polymeric precipitates. Fig. 1 shows that the ELSS microparticles (size range: 100–300 μm) formed as tightly stacked flat and elongated (leaf-shaped) particles. The spontaneous formation of this unique morphology involves the initial aggregation of a crystalline region in the semicrystalline PCL and spherulitic growth during further crystallization (cooling) [23,36,37]. A unique LSS structure has been suggested to provide an appropriate environment for sufficient loading and sustained release of bioactive molecules (e.g., growth factors) to effectively induce cell differentiation [23–26]. Therefore, we presumed that bone regeneration could be induced by loading BMP-2 into ELSS microparticles, which would improve the biofunctional properties of the bioink.

3.2. Preparation of ELSS-loaded SA bioinks and printability testing

After ELSS microparticles had been fabricated, ELSS ink was prepared via mixing with alginate solution (Fig. 1). Alginate is commonly used as a bioink material because of its cell compatibility, cost efficiency, availability, and printability [14]. Although it is generally bioinert, there have been reports of methods that improve its bioactivity for use as a bioink [10,38]. The mixing of alginate with various bioactive materials can synergistically improve the properties of difficult-to-deliver materials, as well as alginate bioactivity [39,40]. In particular, the extrusion-based printing method offers greater flexibility in terms of cell compatibility, compared with other printing methods [41]. Therefore, we evaluated the printability of ELSS ink to investigate the potential for alginate with ELSS microparticles to provide sustained release of growth factor. The printing parameters were adjusted to optimize extrusion printing conditions; specifically, the nozzle gauge was increased (i.e., the needle inner diameter was decreased) from 21G to 23G while the printing pressure was maintained at 100 kPa. Fig. 2A shows that extrusion became more difficult as the ELSS microparticle weight fraction increased because of particle-related nozzle blockage. All groups could be printed with the

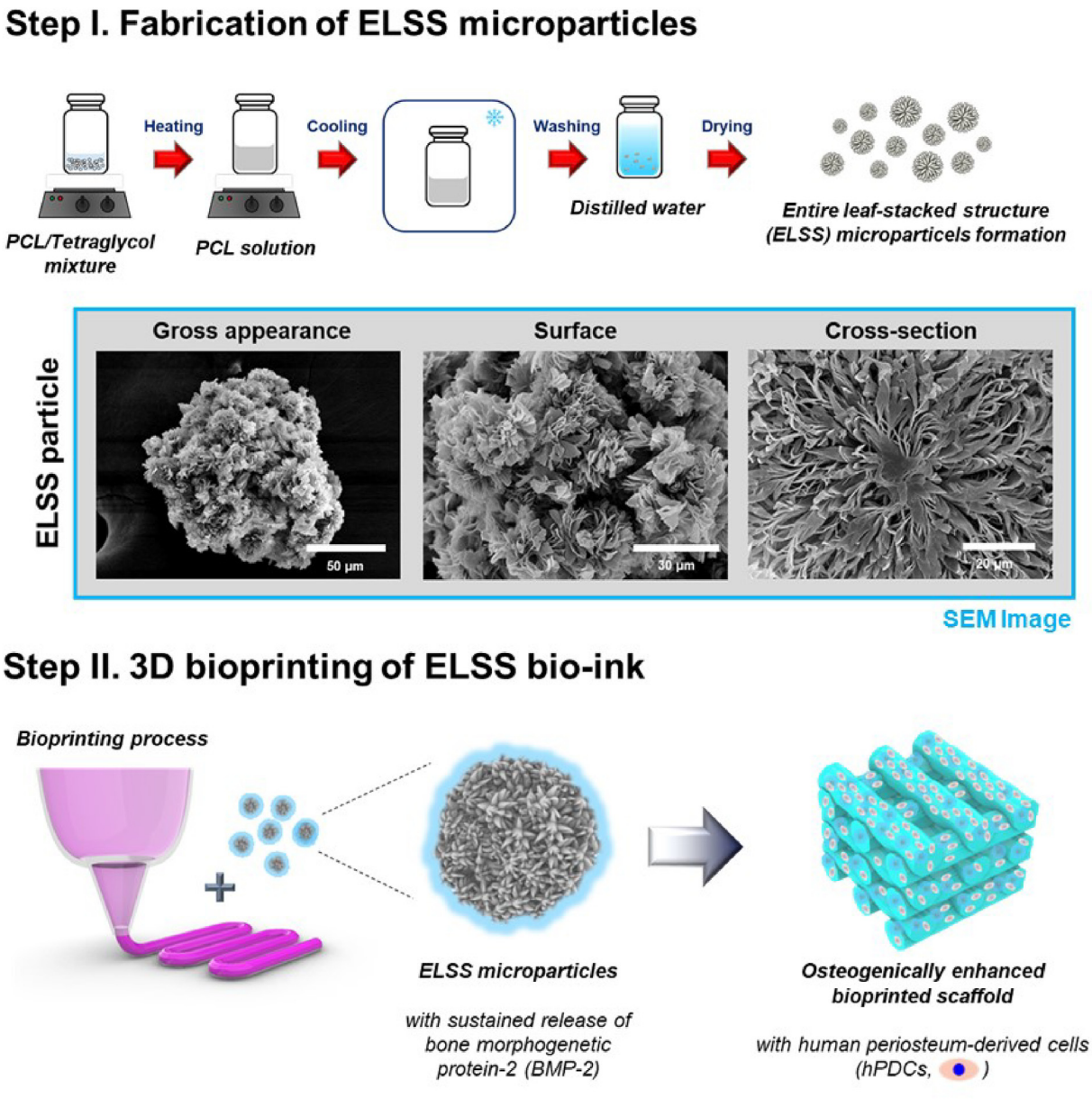

Fig. 1. Illustration of the fabrication of entire leaf-stacked structure (ELSS) microparticles and three-dimensional (3D) bioprinting of ELSS bioink. Blue-outlined box contained scanning electron microscope images of the morphology of fabricated ELSS microparticles. Scale bars of 50, 30, and 20 μm correspond to the gross appearance, surface, and cross-section, respectively. (For interpretation of the references to color in this figure legend, the reader is referred to the Web version of this article.)

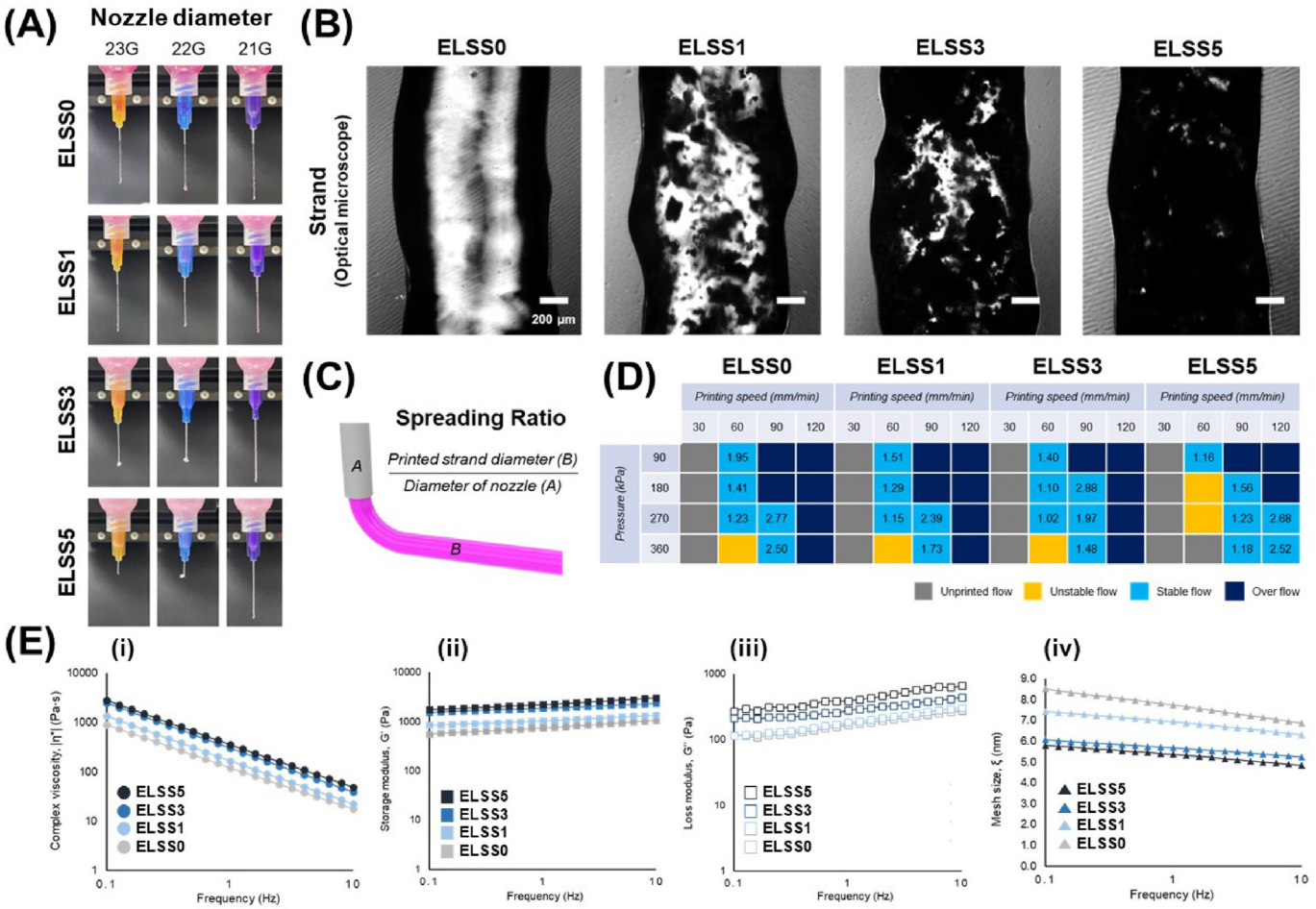

Fig. 2. Printability test and rheological analysis results of the entire leaf-stacked structure (ELSS) ink for microparticle contents of 0, 1, 3, and 5 wt% (corresponding to ELSS0, ELSS1, ELSS3, and ELSS5, respectively). (A) Nozzle gauge was controlled using 21G, 22G, and 23G needles at 100 kPa printing pressure. (B) Optical microscope images of printed strands. Scale bar = 200 μm. (C) Illustration of the spreading ratio of the printed strand. (D) Printability graph according to the spreading ratio of three-dimensionally printed strands: gray = unprinted flow, yellow = unstable flow, light blue = stable flow, dark blue = overflow. (E) Rheological properties of ELSS inks. (i) Complex viscosity (η*), (ii) storage modulus (G′), (iii) loss modulus (G″), and (iv) mean mesh size (ξ). (For interpretation of the references to color in this figure legend, the reader is referred to the Web version of this article.)

larger-bore 21G nozzle with a 500-μm inner diameter; image analysis of the printed strands confirmed that the distribution of ELSS microparticles was uniform (Fig. 2B). After extrudability had been optimized, stable printing conditions were identified by adjusting the printing head speed and the printing pressure (Fig. S1, Fig. 2C and 2D). The spreading ratio was measured using an optical microscope after line printing; a low value indicated that a scaffold structure could be fabricated with high precision [28]. At the preset printing interval, the printed strand structure could be maintained at a spreading ratio of 1–3. Printing became more difficult at low pressure as the particle content increased; compared with hydrogels, the more robust physical properties of mPCL particles prevented stable extrusion. Based on the above results, scaffolds were fabricated with a spreading ratio of 1.2 using ELSS ink.

3.3. Rheological properties of ELSS-loaded SA bioinks

Knowledge of the rheological properties of hydrogels is essential for determining extrusion-based bioink printability [42,43]. The complex viscosity (η*), storage modulus (G′), loss modulus (G″), and mesh size (ξ) were determined using a frequency sweep test from 0.1 to 10 Hz within the linear viscoelastic region (Fig. 2E–H). The η*, G′, and G″ increased as the ELSS particle content increased. The mesh size of the hydrogel network decreased as the particles content increased, consistent with the physical trapping of ELSS microparticles within the hydrogel network, as well as ionic crosslinking [44]. These results confirmed that ELSS microparticle-loaded bioink could be printed and that the physical properties could be modified according to particle content.

3.4. Fabrication of 3D printed scaffolds using ELSS-loaded SA bioinks

Based on the printability and rheological test results, scaffolds were fabricated using a laboratory-made 3D printing system at the Korea Institute of Machinery and Materials. Fig. 3A shows that the fabricated stacked scaffolds could be printed according to the designed size and pattern. Examination of scaffold surface morphology by scanning electron microscopy showed that the printing pattern was controlled by the spreading ratio; the hydrogel pore size decreased with increasing ELSS microparticle content in the ink (Fig. 3B). Importantly, the unique ELSS microparticles maintained their morphology within the scaffold structure after printing, which suggested that sustained drug release could be achieved without further physical/chemical modification. Based on the above results, experiments were conducted to characterize drug-release behavior after printing.

3.5. Profiles of growth factor release from ELSS microparticles and scaffolds

To compare the effects of the concentration of BMP-2 loaded in ELSS

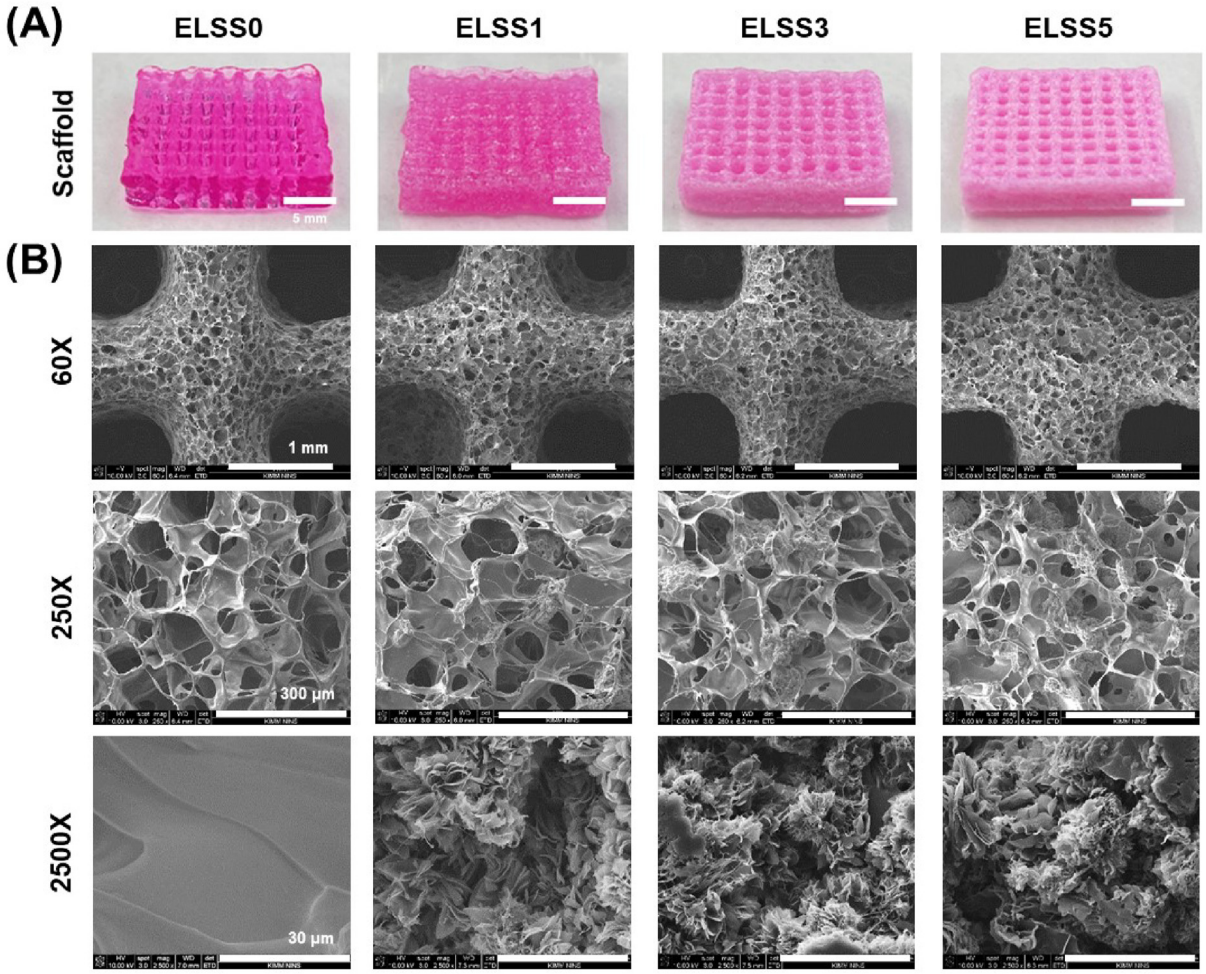

Fig. 3. Fabricated three-dimensionally (3D) printed entire leaf-stacked structure (ELSS) scaffolds. (A) Optical images of ELSS microparticle-loaded three-dimensionally printed scaffolds for ELSS microparticle contents of 0, 1, 3, and 5 wt% (corresponding to ELSS0, ELSS1, ELSS3, and ELSS5, respectively). Scale bars = 5 mm. (B) Scanning electron microscope images of fabricated scaffolds. Scale bars = 1 mm, 300 μm, and 30 μm (corresponding to magnifications of 60 × , 250 × , and 2500 × , respectively).

microparticles, ELSS particles with different loading amounts of BMP-2 were prepared. The loading of BMP-2 in both groups was controlled using different concentrations of BMP-2 (1 and 10 μg/mL). The LSS particles provided a suitable environment to prevent the initial rapid release of BMP-2 from porous particles; BMP-2 was slowly released over 26 days, regardless of the concentration of BMP-2 in the loading solution (1 μg/mL, ~79% of total loading [66.4 ± 0.5 ng/10 mg particles]; 10 μg/mL, ~51% of total loading [313.7 ± 0.2 ng/10 mg particles]) (Fig. 4A). Previous research attributed the continuous release of growth factor from ELSS particles to their repetitive adsorption and desorption as they are released within the complex structure [23–26]. Thus, we expected that ELSS microparticles with different amounts of BMP-2 release could serve as a tool to investigate the effect of BMP-2 concentration on osteogenic differentiation of stem cells in alginate hydrogels.

Chemical interactions between alginate and ELSS microparticles were evaluated using Fourier-transform infrared spectroscopy (Fig. 4B). A broad band at 3100–3600 cm^{-1} (corresponding to the hydroxyl moiety of the SA hydrogel) was evident in all groups; this was consistent with the involvement of alginate in hydrogen bonding and electrostatic interactions with bioactive molecules [17]. In addition, bands at 1294 and 1722 cm^{-1} (corresponding to C–O–C and C═O stretching vibrations, respectively) were increasingly evident with increasing ELSS microparticle content because of the particle composition (PCL) [45]. Additional experiments were conducted to explore the potential for sustained release of growth factor using ELSS microparticles in scaffolds and to measure bioactivity after immobilization to the matrix. Fluorescence-labeled protein-immobilized ELSS microparticles were loaded onto scaffolds to visualize the profiles of bioactive molecule release [46,47]. Fig. 4C shows that FITC-BSA-immobilized ELSS microparticles were present in all printed strands except strands that lacked particles. Microparticle distributions were similar to the distributions in printability tests. As shown in Fig. 5A, the particles released proteins from scaffolds for ≥ 2 weeks, which confirmed that sustained release could be achieved both before and after printing. Furthermore, the fluorescence intensity was also maintained with the increased ratio of the ELSS microparticles for 14 days (Fig. 5B). Therefore, we also expect the bioactivity of BMP-2 is preserved after absorbed to the matrix [48,49]. Especially, the alginate was used to base material for bioprinting with the BMP-2 immobilization to the hydrogel in previous studies [50,51]. However, the group containing only alginate tended to be rapidly degraded in about a week. In addition, the studies of polymeric carrier to delivery BMP-2 for sustained release was difficult to protect denaturation and burst release of the protein [52,53]. To overcome this issues, the printed scaffold structure was maintained through the ionic crosslinking of alginate. Furthermore, the sustained-release profiles were also maintained because of ELSS microparticles immobilized in the ink. We thus concluded that was feasible to fabricate a printing construct that could strongly induce bone regeneration by loading BMP-2 into microparticles.

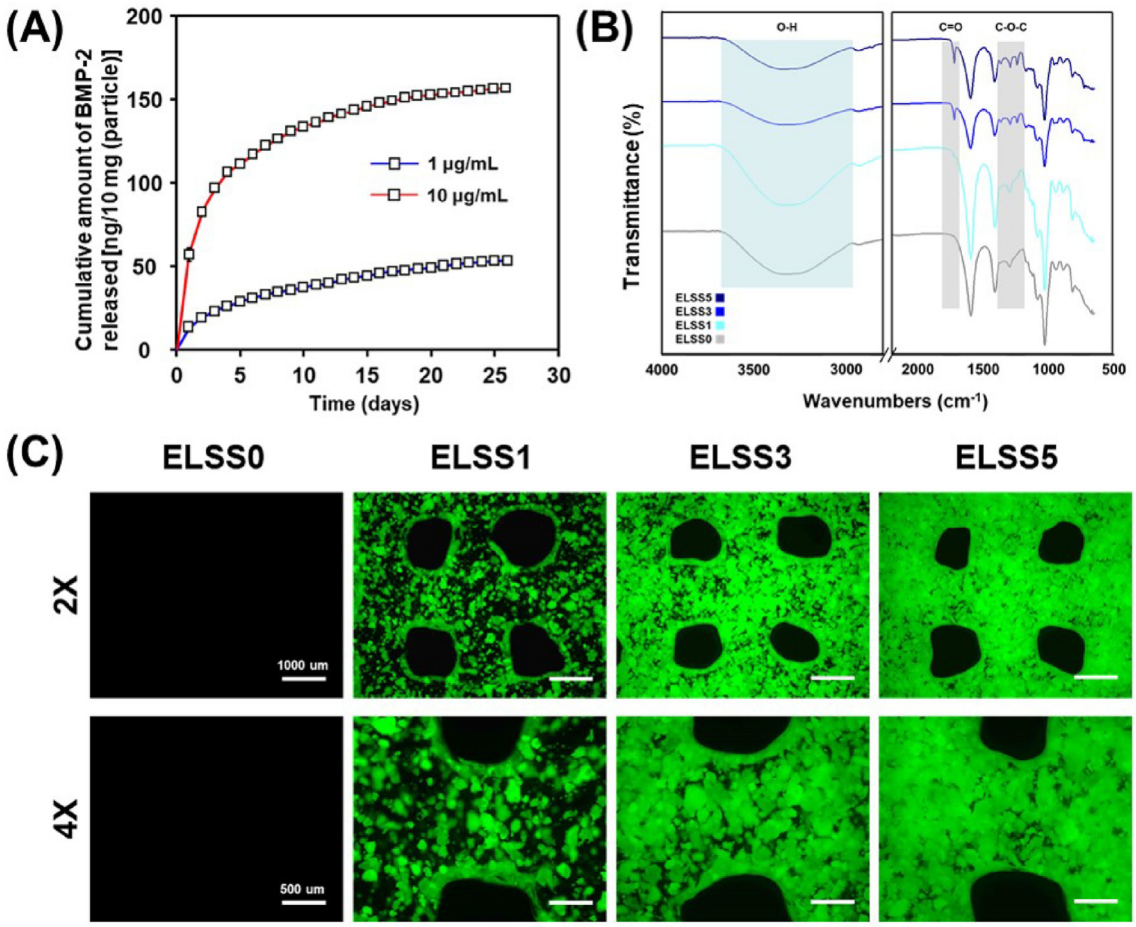

Fig. 4. Profiles of growth factor release from the entire leaf-stacked structure (ELSS) microparticles and scaffolds. (A) Cumulative amounts of BMP-2 released from LSS particles that had been immobilized in different concentrations of loading solution ($n = 3$). (B) Fourier transform-infrared spectra of ELSS inks. (C) Loading of FITC-BSA-immobilized ELSS microparticles into scaffolds. Scale bars = 1000 and 500 μm (corresponding to magnifications of 2 × and 4 × , respectively).

Additional experiments were carried out to determine whether a bioink could provide an environment that was suitable for the differentiation of cells into target cell types.

3.6. Cell viability

The ELSS microparticles maintained their unique structure even after printing; they improved cell adhesion and ensured continuous supply of a bioactive growth factor. However, a previous study showed that the extrusion printing process negatively affected cell viability because of process-induced cell damage under shear stress, which was dependent on printing pressure, nozzle diameter, and length [41]. Consequently, in this study, we used live/dead assays to investigate cell viability in scaffolds that had been fabricated by concurrently printing the ELSS microparticle-loaded bioink and MC-3T3 osteoblast-like cells. The number of dead cells in each scaffold after 24 h increased as the ELSS content increased (Fig. 6A). The cell viability of the ELSS0, ELSS1, ELSS3, and ELSS5 was measured to 91.59 ± 0.47%, 90.09 ± 1.15%, 66.05 ± 4.98%, and 55.97 ± 1.97%, respectively. Because of their more robust mechanical properties compared with pure hydrogel, ELSS particles were expected to cause increasing amounts of cell damage as the ELSS content in bioink increased. In particular, cell damage rapidly occurred at 3 wt%. hPDC viability was examined using groups that contained 0 and 1 wt% ELSS microparticles in bioink (ELSS0 and ELSS1, respectively; Fig. 6B and C). The ELSS0 and ELSS1 groups exhibited respective cell viabilities of 91.46 ± 4.08% and 91.51 ± 1.75% on day 1, and 86.50 ± 1.62% and 87.83 ± 6.59% on day 7; there were no significant differences between the two groups. In addition, cell viability over 7 days was stable at > 85% in both groups. These results confirmed successful bioprinting of ELSS bioink with hPDCs. This bioprinting method could release BMP-2 in a sustained-release manner without physical/chemical modification; the system can print loaded cells without negatively affecting cell viability. Based on the cell viability test results, we next evaluated the osteogenic differentiation and mineralization of hPDCs encapsulated in scaffolds.

3.7. Osteogenic differentiation and mineralization of hPDCs

BMP-2 is widely used as a clinical alternative to autologous bone for regenerative approaches that require osteogenic differentiation. However, the current delivery carrier (collagen-type) has limitations related to the rapid release of growth factor and inadequate mechanical properties [20,54]. Here, we found that sustained release of BMP-2 was maintained over 4 weeks through the immobilization of BMP-2 on ELSS microparticles, followed by nontoxic bioprinting of hPDCs. Osteogenic differentiation of hPDCs by BMP-2-loaded ELSS microparticles was evaluated by comparing the behaviors of the ELSS0 and ELSS1 groups over 2 weeks due to the challenge for maintaining the printed structure when relying solely on alginate-based bioprinting [55,56]. Relative ALP activity was analyzed using *p*-nitrophenyl phosphate as a substrate indicative of ALP to evaluate the benefits of BMP-2 immobilized to the ELSS microparticles (Fig. 7A).

After normalization to the values on day 7, the ELSS1 group demonstrated increased osteogenic differentiation on day 14, compared with the ELSS0 group. Calcium deposition is a reliable marker of

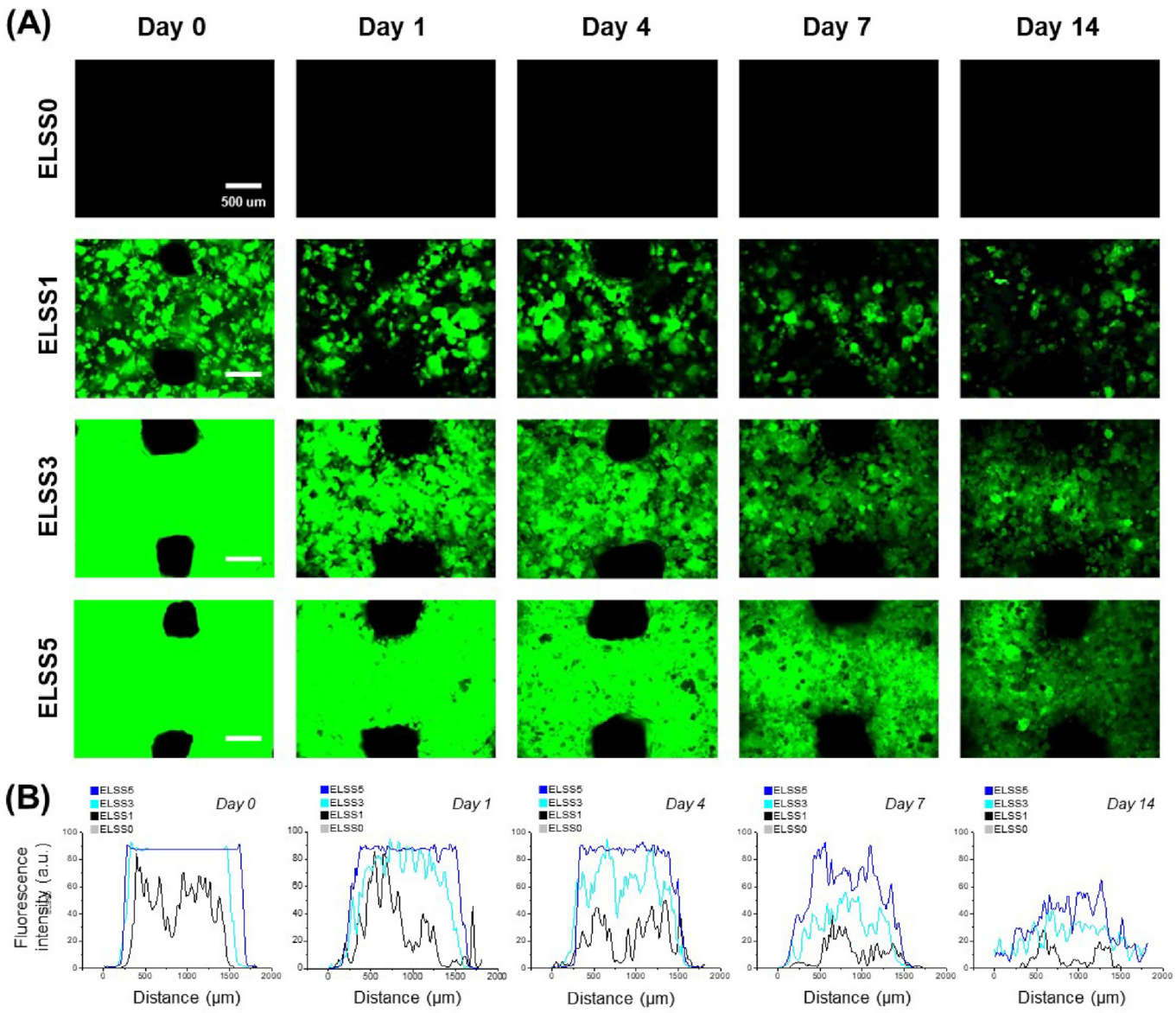

Fig. 5. Fluorescent analysis (A) Analysis of protein release from FITC-BSA-immobilized entire leaf-stacked structure (ELSS) microparticle-loaded ink over 2 weeks; Scale bars = 500 μm. (B) Fluorescence intensity measurements according to the distance in the strand of the scaffold (μm).

osteogenic differentiation; calcium deposition in hPDCs was assessed by calcium colorimetric assay (Fig. 7B). Higher calcium content was observed in the ELSS1 group that contained BMP-2-immobilized ELSS particles; this finding was consistent with the difference in ALP activity between the ELSS0 and ELSS1 groups. Cell mineralization, which constitutes the deposition of bone-like nodules in cells, was evaluated by hydroxyapatite staining; nuclei were stained with DAPI (Fig. 7C) [57]. hPDC-mediated hydroxyapatite appeared green; it was more common in the ELSS1 group that contained ELSS microparticles. Furthermore, Alizarin Red staining was performed to examine the calcium mineralization of hPDCs. The extent of red color was greater in the ELSS1 group than in the ELSS0 group, suggesting that the inclusion of ELSS microparticles led to osteogenic differentiation and mineralization of hPDCs in ELSS bioink. Notably, markers of early- and late-stage osteogenesis were increased in the ELSS1 group compared with the ELSS0 group, as demonstrated by ALP activity and calcium deposition in hPDCs [58,59]. In addition, hPDC mineralization was promoted by the sustained release of BMP-2 that had been immobilized in ELSS particles in the bioink. Based on this, we anticipate to the potential to create a model that can be applied to actual therapy in the future.

3.8. Immunocytochemical analysis of Runx2 of hPDCs

The differentiation behavior of BMP-2-stimulated hPDCs in alginate hydrogels was examined by staining with antibodies against Runx2, which is a well-known specific marker of osteogenic differentiation [60]. The signal of the Runx2 marker (green) gradually increased over time in all groups, but green fluorescence was more clearly detected in the ELSS1 group than in the ELSS0 group. This indicated that continuous supply of BMP-2 promoted the osteogenic differentiation of hPDCs (Fig. 8). This finding is similar to the results regarding osteogenic differentiation and mineralization of hPDCs, suggesting that microsized particle printing is feasible for clinical applications where sustained release of growth factor is needed for bone regeneration. Our enhanced bioprinting process involving biofunctional microparticles could be used to fabricate scaffolds that continuously release drugs according to the amount of drug loaded. This offers an alternative strategy for growth factor therapy, which requires large amounts because growth factors are rapidly inactivated and removed from the target tissue. In addition, local and targeted drug delivery could be achieved using 3D printing technology to mimic the environments of tissue defects that require treatment. We

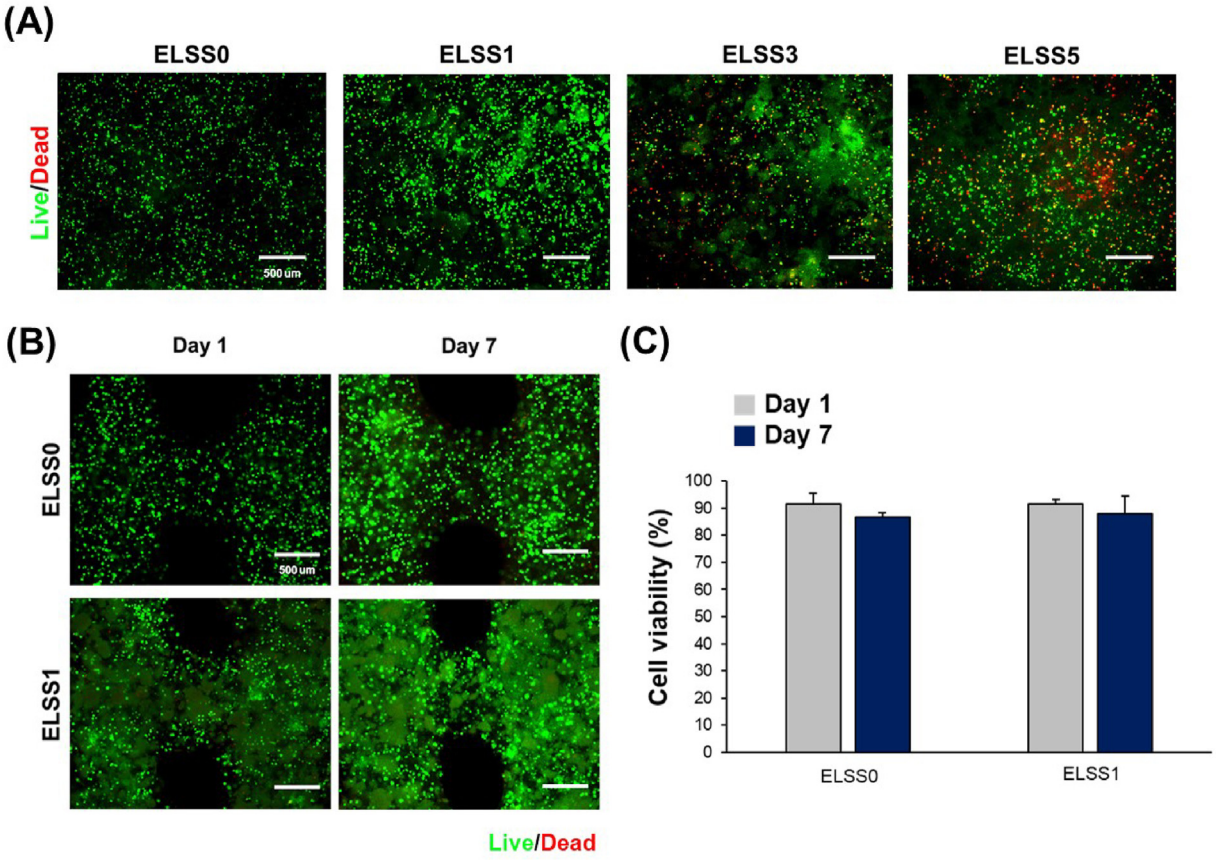

Fig. 6. Analyses of cell viability in entire leaf-stacked structure (ELSS) bioinks. (A) Live/dead assays of cells in bioprinted ELSS scaffolds: MC-3T3 cells over 24 h and (B) hPDCs over 7 days. (C) Viabilities of hPDCs in the ELSS0 and ELSS1 scaffolds on days 1 and 7; initial cell densities were 2×10^6 cells/mL in both groups. Scale bars = 500 μm.

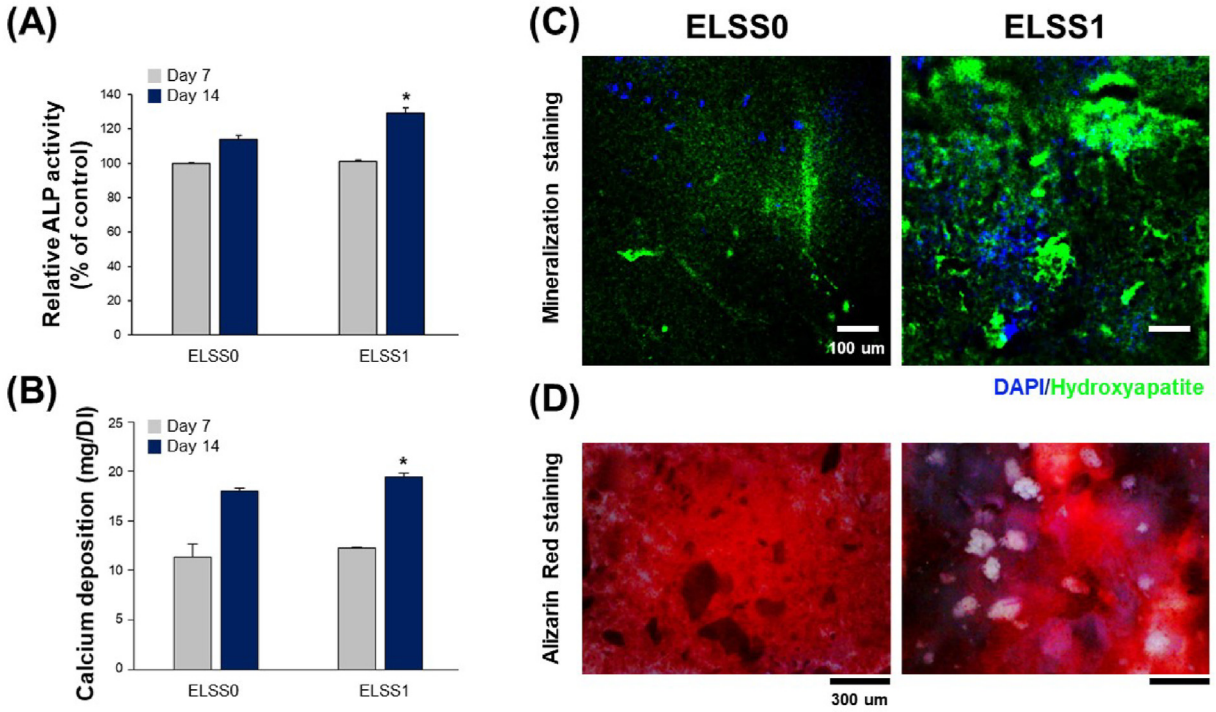

Fig. 7. Osteogenic differentiation and mineralization of hPDCs in the ELSS0 and ELSS1 scaffolds. (A) Quantitative analysis of ALP activity on days 7 and 14. (B) Quantitative analysis of calcium deposition on days 7 and 14; n = 3, * all were significantly different ($p < 0.05$) from ELSS0 on both days. (C) Hydroxyapatite staining assay on day 14; green = hydroxyapatite, blue = cell nuclei. Scale bars = 100 μm. (D) Alizarin Red staining analysis on day 14. Scale bars = 300 μm. (For interpretation of the references to color in this figure legend, the reader is referred to the Web version of this article.)

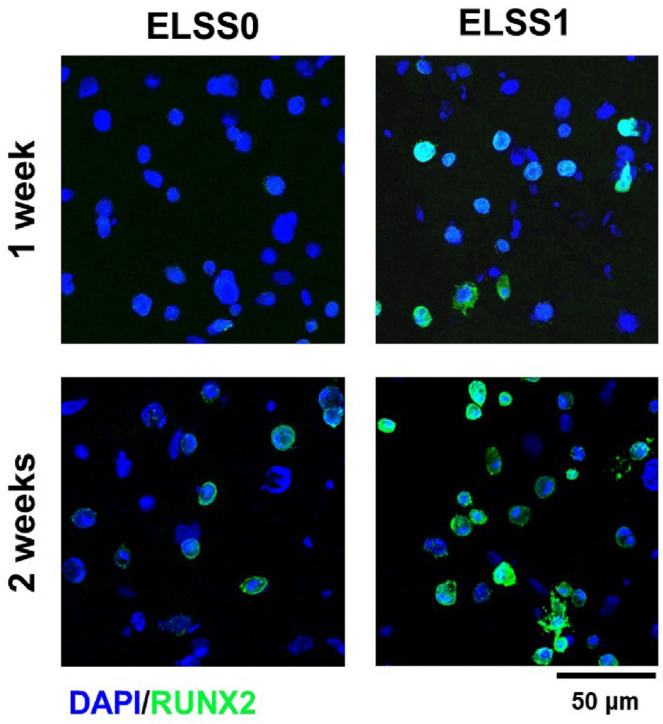

Fig. 8. Expression of osteogenic differentiation marker; green = Runx2, blue = cell nuclei. Scale bars = 50 μm. (For interpretation of the references to color in this figure legend, the reader is referred to the Web version of this article.)

expect that a clinically acceptable system will be achieved by combining various biocompatible hydrogels and bioactive materials loaded on ELSS particles.

4. Conclusions

We have developed a novel strategy for the delivery of bioactive molecules using extrusion printing. Notably, the incorporation of LSS microparticles into a 3D bioink with hPDCs enabled the sustained release of BMP-2 without physical/chemical changes. Through printability testing and rheological analysis, the ratio of hydrogel and ELSS particles was optimized to achieve an ink composition suitable for printing. Although the mechanical properties of the ink improved with increasing particle content, the shear stress developed during printing affected cell viability; conditions that did not affect cell viability were identified. Additionally, *in vitro* experiments revealed that osteogenic differentiation and mineralization of hPDCs were improved in printed scaffolds, with better survival in the group that contained ELSS particles. Our findings offer a novel alternative therapy for bone regeneration treatment that involves 3D bioprinting and sustained-release microparticles constructed with clinically acceptable materials.

CRediT authorship contribution statement

Ji Min Seok: Writing – original draft, Conceptualization. **Min Ji Kim:** Writing – original draft, Methodology. **Jin Ho Park:** Methodology, Formal analysis. **Dahong Kim:** Methodology, Formal analysis. **Dongjin Lee:** Methodology, Formal analysis. **Seon Ju Yeo:** Investigation, Resources. **Jun Hee Lee:** Investigation, Resources. **Kangwon Lee:** Investigation, Resources. **June-Ho Byun:** Supervision. **Se Heang Oh:** Supervision. **Su A Park:** Writing – review & editing, Supervision.

Declaration of competing interest

The authors declare that they have no known competing financial interests or personal relationships that could have appeared to influence the work reported in this paper.

Data availability

No data was used for the research described in the article.

Acknowledgment

This research was supported by the National Research Foundation (NRF; No. NRF-2019M3A9E2066348) and the National Research Council of Science & Technology (NST; CRC22021-200).

Appendix A. Supplementary data

Supplementary data related to this article can be found at https://doi.org/10.1016/j.mtbio.2023.100685.

References

[1] A.C. Daly, M.E. Prendergast, A.J. Hughes, J.A. Burdick, Bioprinting for the biologist, Cell 184 (2021) 18–32, https://doi.org/10.1016/j.cell.2020.12.002.
[2] F. Stapenhorst, M. Garrido dos Santos, J.P. Prestes, B.J. Alcantara, M. Felisberto Borges, P. Pranke, Bioprinting: a promising approach for tissue regeneration, Bioprinting 22 (2021), e00130, https://doi.org/10.1016/j.bprint.2021.e00130.
[3] S. Vanaei, M.S. Parizi, S. Vanaei, F. Salemizadehparizi, H.R. Vanaei, An overview on materials and techniques in 3D bioprinting toward biomedical application, Eng. Regen. 2 (2021) 1–18, https://doi.org/10.1016/j.engreg.2020.12.001.
[4] A.C. Fonseca, F.P.W. Melchels, M.J.S. Ferreira, S.R. Moxon, G. Potjewyd, T.R. Dargaville, S.J. Kimber, M. Domingos, Emulating human tissues and organs: a bioprinting perspective toward personalized medicine, Chem. Rev. 120 (2020) 11093–11139, https://doi.org/10.1021/acs.chemrev.0c00342.
[5] J. Gopinathan, I. Noh, Recent trends in bioinks for 3D printing, Biomater. Res. 22 (2018) 11, https://doi.org/10.1186/s40824-018-0122-1.
[6] T. Zhang, W. Zhao, Z. Xiahou, X. Wang, K. Zhang, J. Yin, Bioink design for extrusion-based bioprinting, Appl. Mater. Today 25 (2021), 101227, https://doi.org/10.1016/j.apmt.2021.101227.
[7] F. Fazal, S. Raghav, A. Callanan, V. Koutsos, N. Radacsi, Recent advancements in the bioprinting of vascular grafts, Biofabrication 13 (2021), 032003, https://doi.org/10.1088/1758-5090/ac0963.
[8] J.M. Fernández-Costa, X. Fernández-Garibay, F. Velasco-Mallorquí, J. Ramón-Azcón, Bioengineered in vitro skeletal muscles as new tools for muscular dystrophies preclinical studies, J. Tissue Eng. 12 (2021) 1–19, https://doi.org/10.1177/2041731420981339.
[9] Y. Chu, L. Huang, W. Hao, T. Zhao, H. Zhao, W. Yang, X. Xie, L. Qian, Y. Chen, J. Dai, Long-term stability, high strength, and 3D printable alginate hydrogel for cartilage tissue engineering application, Biomed. Mater. 16 (2021), 064102, https://doi.org/10.1088/1748-605X/ac2595.
[10] C.C. Piras, D.K. Smith, Multicomponent polysaccharide alginate-based bioinks, J. Mater. Chem. B 8 (2020) 8171–8188, https://doi.org/10.1039/d0tb01005g.
[11] A. Liberski, N. Latif, C. Raynaud, C. Bollensdorff, M. Yacoub, Alginate for cardiac regeneration: from seaweed to clinical trials, Glob. Cardiol. Sci. Pract. 4 (2016), https://doi.org/10.21542/gcsp.2016.4.
[12] J. Lee, J. Hong, W.J. Kim, G.H. Kim, Bone-derived dECM/alginate bioink for fabricating a 3D cell-loaded mesh structure for bone tissue engineering, Carbohydr. Polym. 250 (2020), 116914, https://doi.org/10.1016/j.carbpol.2020.116914.
[13] J. Jia, D.J. Richards, S. Pollard, Y. Tan, J. Rodriguez, R.P. Visconti, T.C. Trusk, M.J. Yost, H. Yao, R.R. Markwald, Y. Mei, Engineering alginate as bioink for bioprinting, Acta Biomater. 10 (2014) 4323–4331, https://doi.org/10.1016/j.actbio.2014.06.034.
[14] Q. Gao, B.S. Kim, G. Gao, Advanced strategies for 3D bioprinting of tissue and organ analogs using alginate hydrogel bioinks, Mar. Drugs 19 (2021) 708, https://doi.org/10.3390/md19120708.
[15] J.H. Kim, J.J. Yoo, S.J. Lee, Three-dimensional cell-based bioprinting for soft tissue regeneration, Tissue Eng. Regenerat. Med. 13 (2016) 647–662, https://doi.org/10.1007/s13770-016-0133-8.
[16] R. Ahmad Raus, W.M.F. Wan Nawawi, R.R. Nasaruddin, Alginate and alginate composites for biomedical applications, Asian J. Pharm. Sci. 16 (2021) 280–306, https://doi.org/10.1016/j.ajps.2020.10.001.
[17] S. Mallakpour, E. Azadi, C.M. Hussain, State-of-the-art of 3D printing technology of alginate-based hydrogels–An emerging technique for industrial applications, Adv. Colloid Interface Sci. 293 (2021), 102436, https://doi.org/10.1016/j.cis.2021.102436.
[18] J. Venkatesan, I. Bhatnagar, P. Manivasagan, K.H. Kang, S.K. Kim, Alginate composites for bone tissue engineering: a review, Int. J. Biol. Macromol. 72 (2015) 269–281, https://doi.org/10.1016/j.ijbiomac.2014.07.008.
[19] G.L. Koons, M. Diba, A.G. Mikos, Materials design for bone-tissue engineering, Nat. Rev. Mater. 5 (2020) 584–603, https://doi.org/10.1038/s41578-020-0204-2.

[20] T.M. De Witte, L.E. Fratila-Apachitei, A.A. Zadpoor, N.A. Peppas, Bone tissue engineering via growth factor delivery: from scaffolds to complex matrices, Regen. Biomater. 5 (2018) 197–211, https://doi.org/10.1093/rb/rby013.

[21] X. Chen, B. Tan, Z. Bao, S. Wang, R. Tang, Z. Wang, G. Chen, S. Chen, W.W. Lu, D. Yang, S. Peng, Enhanced bone regeneration via spatiotemporal and controlled delivery of a genetically engineered BMP-2 in a composite hydrogel, Biomaterials 277 (2021), 121117, https://doi.org/10.1016/j.biomaterials.2021.121117.

[22] A.M. Vargason, A.C. Anselmo, S. Mitragotri, The evolution of commercial drug delivery technologies, Nat. Biomed. Eng. 5 (2021) 951–967, https://doi.org/10.1038/s41551-021-00698-w.

[23] H.Y. Kim, J.H. Lee, H.A.R. Lee, J.S. Park, D.K. Woo, H.C. Lee, G.J. Rho, J.H. Byun, S.H. Oh, Sustained release of BMP-2 from porous particles with leaf-stacked structure for bone regeneration, ACS Appl. Mater. Interfaces 10 (2018) 21091–21102, https://doi.org/10.1021/acsami.8b02141.

[24] H.Y. Kim, B.S. An, M.J. Kim, Y.J. Jeoung, J.H. Byun, J.H. Lee, S.H. Oh, Signaling molecule-immobilized porous particles with a leaf-stacked structure as a bioactive filler system, ACS Biomater. Sci. Eng. 6 (2020) 2231–2239, https://doi.org/10.1021/acsbiomaterials.9b01731.

[25] M.J. Kim, J.H. Lee, J.S. Kim, H.Y. Kim, H.C. Lee, J.H. Byun, J.H. Lee, N.H. Kim, S.H. Oh, Intervertebral disc regeneration using stem cell/growth factor-loaded porous particles with a leaf-stacked structure, Biomacromolecules 21 (2020) 4795–4805, https://doi.org/10.1021/acs.biomac.0c00992.

[26] M.J. Kim, Y.J. Jeoung, H.Y. Kim, S.Y. Kim, J.Y. Kim, J.W. Park, J.H. Byun, J.H. Lee, S.H. Oh, Cell spheroids containing bioactive molecule-immobilized porous particles with a leaf-stacked structure, Chem. Eng. J. 429 (2022), 132590, https://doi.org/10.1016/j.cej.2021.132590.

[27] S. Im, G. Choe, J.M. Seok, S.J. Yeo, J.H. Lee, W.D. Kim, J.Y. Lee, S.A. Park, An osteogenic bioink composed of alginate, cellulose nanofibrils, and polydopamine nanoparticles for 3D bioprinting and bone tissue engineering, Int. J. Biol. Macromol. 205 (2022) 520–529, https://doi.org/10.1016/j.ijbiomac.2022.02.012.

[28] F.E. Freeman, D.J. Kelly, Tuning alginate bioink stiffness and composition for controlled growth factor delivery and to spatially direct MSC fate within bioprinted tissues, Sci. Rep. 7 (2017), 17042, https://doi.org/10.1038/s41598-017-17286-1.

[29] Y. Gan, P. Li, L. Wang, X. Mo, L. Song, Y. Xu, C. Zhao, B. Ouyang, B. Tu, L. Luo, L. Zhu, S. Dong, F. Li, Q. Zhou, An interpenetrating network-strengthened and toughened hydrogel that supports cell-based nucleus pulposus regeneration, Biomaterials 136 (2017) 12–28, https://doi.org/10.1016/j.biomaterials.2017.05.017.

[30] M. Kisiel, A.S. Klar, M. Ventura, J. Buijs, M.K. Mafina, S.M. Cool, J. Hilborn, Complexation and sequestration of BMP-2 from an ECM mimetic hyaluronan gel for improved bone formation, PLoS One 8 (2013), e78551, https://doi.org/10.1371/journal.pone.0078551.

[31] S.J. Lee, J.M. Seok, J.H. Lee, J. Lee, W.D. Kim, S.A. Park, Three-dimensional printable hydrogel using a hyaluronic acid/sodium alginate bio-ink, Polymers 13 (2021) 1–8, https://doi.org/10.3390/polym13050794.

[32] J. Park, S.J. Lee, S. Chung, J.H. Lee, W.D. Kim, J.Y. Lee, S.A. Park, Cell-laden 3D bioprinting hydrogel matrix depending on different compositions for soft tissue engineering: characterization and evaluation, Mater. Sci. Eng., C 71 (2017) 678–684, https://doi.org/10.1016/j.msec.2016.10.069.

[33] Y.H. Shen, M.S. Shoichet, M. Radisic, Vascular endothelial growth factor immobilized in collagen scaffold promotes penetration and proliferation of endothelial cells, Acta Biomater. 4 (2008) 477–489, https://doi.org/10.1016/j.actbio.2007.12.011.

[34] D.K. Yoon, J.S. Park, G.J. Rho, H.J. Lee, I.Y. Sung, J.H. Son, B.W. Park, Y.H. Kang, S.H. Byun, S.C. Hwang, D.K. Woo, Y.C. Cho, J.H. Byun, The involvement of histone methylation in osteoblastic differentiation of human periosteum-derived cells cultured *in vitro* under hypoxic conditions, Cell Biochem. Funct. 35 (2017) 441–452, https://doi.org/10.1002/cbf.3302.

[35] H.Y. Kim, S.Y. Kim, H.Y. Lee, J.H. Lee, G.J. Rho, H.J. Lee, H.C. Lee, J.H. Byun, S.H. Oh, Oxygen-releasing microparticles for cell survival and differentiation ability under hypoxia for effective bone regeneration, Biomacromolecules 20 (2019) 1087–1097, https://doi.org/10.1021/acs.biomac.8b01760.

[36] A.G.A. Coombes, S.C. Rizzi, M. Williamson, J.E. Barralet, S. Downes, W.A. Wallace, Precipitation casting of polycaprolactone for applications in tissue engineering and drug delivery, Biomaterials 25 (2004) 315–325, https://doi.org/10.1016/S0142-9612(03)00535-0.

[37] M. Kuterbekov, P. Machillot, P. Lhuissier, C. Picart, A.M. Jonas, K. Glinel, Solvent-free preparation of porous poly(L-lactide) microcarriers for cell culture, Acta Biomater. 75 (2018) 300–311, https://doi.org/10.1016/j.actbio.2018.06.009.

[38] K. Markstedt, A. Mantas, I. Tournier, H. Martínez Ávila, D. Hägg, P. Gatenholm, 3D bioprinting human chondrocytes with nanocellulose-alginate bioink for cartilage tissue engineering applications, Biomacromolecules 16 (2015) 1489–1496, https://doi.org/10.1021/acs.biomac.5b00188.

[39] S.K. Leslie, A.M. Nicolini, G. Sundaresan, J. Zweit, B.D. Boyan, Z. Schwartz, Development of a cell delivery system using alginate microbeads for tissue regeneration, J. Mater. Chem. B 4 (2016) 3515–3525, https://doi.org/10.1039/c6tb00035e.

[40] H.H. Tønnesen, J. Karlsen, Alginate in drug delivery systems, Drug Dev. Ind. Pharm. 28 (2002) 621–630, https://doi.org/10.1081/DDC-120003853.

[41] M. Askari, M. Afzali Naniz, M. Kouhi, A. Saberi, A. Zolfagharian, M. Bodaghi, Recent progress in extrusion 3D bioprinting of hydrogel biomaterials for tissue regeneration: a comprehensive review with focus on advanced fabrication techniques, Biomater. Sci. 9 (2021) 535–573, https://doi.org/10.1039/d0bm00973c.

[42] M. Chopin-Doroteo, E.A. Mandujano-Tinoco, E. Krötzsch, Tailoring of the rheological properties of bioinks to improve bioprinting and bioassembly for tissue replacement, Biochim. Biophys. Acta Gen. Subj. 1865 (2020), 129782, https://doi.org/10.1016/j.bbagen.2020.129782.

[43] M.E. Cooke, D.H. Rosenzweig, The rheology of direct and suspended extrusion bioprinting, APL Bioeng 5 (2021), 011502, https://doi.org/10.1063/5.0031475.

[44] M. Fenbo, L. Sijing, L.I. Ruiz-Ortega, Z. Yuanjun, X. Lei, W. Kui, L. Lijun, T. Bin, Effects of alginate/chondroitin sulfate-based hydrogels on bone defects healing, Mater. Sci. Eng. C 116 (2020), 111217, https://doi.org/10.1016/j.msec.2020.111217.

[45] A. Valizadeh, A. Abdollahi, N. Ranjbar, H.R. Kelidari, H. Sereshti, M. Osanloo, Antibacterial effects of impregnated scaffolds with solid lipid nanoparticles gels containing three essential oils against standard and clinical strains of *Pseudomonas aeruginosa* and *Staphylococcus aureus*, Nanomedicine Res. J. 6 (2021) 218–227, https://doi.org/10.22034/nmrj.2021.03.002.

[46] C. Wischke, H.H. Borchert, Fluorescein isothiocyanate labelled bovine serum albumin (FITC-BSA) as a model protein drug: opportunities and drawbacks, Pharmazie 61 (2006) 770–774.

[47] J. Lommen, L. Schorn, A. Landers, H. Holtmann, K. Berr, N.R. Kübler, C. Sproll, M. Rana, R. Depprich, Release kinetics of the model protein FITC-BSA from different polymer-coated bovine bone substitutes, Head Face Med. 15 (2019) 1–13, https://doi.org/10.1186/s13005-019-0211-y.

[48] J.J. Patel, C.L. Flanagan, S.J. Hollister, Bone morphogenetic protein-2 adsorption onto poly-ε-caprolactone better preserves bioactivity in vitro and produces more bone in vivo than conjugation under clinically relevant loading scenarios, Tissue Eng. C Methods 21 (2015) 489–498, https://doi.org/10.1089/ten.tec.2014.0377.

[49] Y.P. Yun, J.Y. Lee, W.J. Jeong, K. Park, H.J. Kim, J.J. Song, S.E. Kim, H.R. Song, Improving osteogenesis activity on BMP-2-immobilized PCL fibers modified by the γ -ray irradiation technique, BioMed Res. Int. 2015 (2015), 302820, https://doi.org/10.1155/2015/302820.

[50] M.T. Poldervaart, H. Wang, J. Van Der Stok, H. Weinans, S.C.G. Leeuwenburgh, F.C. Oner, W.J.A. Dhert, J. Alblas, Sustained release of BMP-2 in bioprinted alginate for osteogenicity in mice and rats, PLoS One 8 (2013), https://doi.org/10.1371/journal.pone.0072610.

[51] Y.M. Kolambkar, K.M. Dupont, J.D. Boerckel, N. Huebsch, D.J. Mooney, D.W. Hutmacher, R.E. Guldberg, An alginate-based hybrid system for growth factor delivery in the functional repair of large bone defects, Biomaterials 32 (2011) 65–74, https://doi.org/10.1016/j.biomaterials.2010.08.074.

[52] C. Whitty, C. Pernstich, C. Marris, A. McCaskie, M. Jones, F. Henson, Sustained delivery of the bone morphogenetic proteins BMP-2 and BMP-7 for cartilage repair and regeneration in osteoarthritis, Osteoarthr. Cartil. Open. 4 (2022), 100240, https://doi.org/10.1016/j.ocarto.2022.100240.

[53] V. Agrawal, M. Sinha, A review on carrier systems for bone morphogenetic protein-2, J. Biomed. Mater. Res. Part B Appl. Biomater. 105 (2017) 904–925, https://doi.org/10.1002/jbm.b.33599.

[54] E. Wawrzyńska, D. Kubies, Alginate matrices for protein delivery - a short review, Physiol. Res. 67 (2018) s319–s334, https://doi.org/10.33549/physiolres.933980.

[55] S. Murab, A. Gupta, M.K. Włodarczyk-Biegun, A. Kumar, P. van Rijn, P. Whitlock, S.S. Han, G. Agrawal, Alginate based hydrogel inks for 3D bioprinting of engineered orthopedic tissues, Carbohydr. Polym. 296 (2022), 119964, https://doi.org/10.1016/j.carbpol.2022.119964.

[56] T. Gonzalez-Fernandez, A.J. Tenorio, K.T. Campbell, E.A. Silva, J.K. Leach, Alginate-based bioinks for 3D bioprinting and fabrication of anatomically accurate bone grafts, Tissue Eng. 27 (2021) 1168–1181, https://doi.org/10.1089/ten.tea.2020.0305.

[57] K. Vuornos, H. Huhtala, M. Kääriäinen, K. Kuismanen, L. Hupa, M. Kellomäki, S. Miettinen, Bioactive glass ions for *in vitro* osteogenesis and microvascularization in gellan gum-collagen hydrogels, J. Biomed. Mater. Res. Part B. Appl. Biomater. 108 (2020) 1332–1342, https://doi.org/10.1002/jbm.b.34482.

[58] J. Eyckmans, G.L. Lin, C.S. Chen, Adhesive and mechanical regulation of mesenchymal stem cell differentiation in human bone marrow and periosteum-derived progenitor cells, Biol. Open. 1 (2012) 1058–1068, https://doi.org/10.1242/bio.20122162.

[59] Y.P. Yun, S.Y. Lee, H.J. Kim, J.J. Song, S.E. Kim, Improvement of osteoblast functions by sustained release of bone morphogenetic protein-2 (BMP-2) from heparin-coated chitosan scaffold, Tissue Eng. Regen. Med. 10 (2013) 183–191, https://doi.org/10.1007/s13770-013-0389-1.

[60] A.R. Costa-Pinto, V.M. Correlo, P.C. Sol, M. Bhattacharya, P. Charbord, B. Delorme, R.L. Reis, N.M. Neves, Osteogenic differentiation of human bone marrow mesenchymal stem cells seeded on melt-based chitosan scaffolds for bone tissue engineering applications, Biomacromolecules 10 (2009) 2067–2073, https://doi.org/10.1021/bm9000102.